

Thermal Decomposition of Crystalline Ni^{II}–Cr^{III} Layered Double Hydroxide: A Structural Study of the Segregation Process

Elsa E. Sileo,^{*,†} Matías Jobbágy,^{*,†} Carlos O. Paiva-Santos,[‡] and Alberto E. Regazzoni[§]

INQUIMAE, Facultad de Ciencias Exactas y Naturales, Universidad de Buenos Aires, Pabellón II, Ciudad Universitaria, C1428EHA - Buenos Aires, Argentina, Instituto de Química, Universidade Estadual Paulista, UNESP, Araraquara, 14801–970, São Paulo, Brazil, and Unidad de Actividad Química, Comisión Nacional de Energía Atómica, Centro Atómico Constituyentes, Avenida General Paz 1499, B1650KNA - San Martín (Pcia. de Buenos Aires), Argentina

Received: February 4, 2005; In Final Form: March 29, 2005

A structural study of the thermal evolution of Ni_{0.69}Cr_{0.31}(OH)₂(CO₃)_{0.155}·*n*H₂O into NiO and tetragonal NiCr₂O₄ is reported. The characteristic structural parameters of the two coexisting crystalline phases, as well as their relative abundance, were determined by Rietveld refinement of powder x-ray diffraction (PXRD) patterns. The results of the simulations allowed us to elucidate the mechanism of the demixing process of the oxides. It is demonstrated that nucleation of a metastable nickel chromite within the common oxygen framework of the parent Cr^{III}-doped bunsenite is the initial step of the cationic redistribution. The role that trivalent cations play in the segregation of crystalline spinels is also discussed.

1. Introduction

Layered double hydroxides (LDHs), of general formula, M_{1-x}^{II}M_x^{III}(OH)₂A_{x/m}·*n*H₂O, are lamellar, brucite-like, mixed hydroxides where M^{II} cations are partially substituted by the M^{III} ones; commonly, substitution degrees range between 0.33 and 0.20, expressed as cation molar fraction.¹ The anions A^{m-} occupy the interlamellar space and counterbalance the excess of positive charge due to the substitution. If the interlamellar anions are volatile species such as carbonate or nitrate, thermal decomposition of LDHs easily leads to mixed M^{II}, M^{III} oxides at significant lower temperatures and shorter times than traditional ceramic procedures.^{2–6} In addition, the chemical decomposition (CD) route,⁷ which involves moderate annealing, allows one to preserve (or even increase) the surface area of the starting precursor.⁸ This characteristic is highly appreciated in the field of heterogeneous catalysis, where the crystalline and chemical properties, as well as the textural ones, are crucial.^{9–17} Many interesting materials have been obtained upon thermal decomposition of LDHs, ranging from multicationic oxides^{18,19} to novel single-phase spinels.²⁰

Despite the large number of reports concerning the thermal decomposition of LDHs, many structural aspects related to the crystallization of the mixed oxides during annealing still remain obscure, mostly because the presence of amorphous phases blurs traditional PXRD analysis.²¹ However, certain LDHs, such as Ni_{1-x}Cr_x(OH)₂(CO₃)_{x/2}·*n*H₂O, decompose into crystalline mixed oxides at relatively low temperatures,²² providing a suitable system to explore.

Here, we report, using Rietveld refinement, the structural features associated with the solid-state transformation during the thermal decomposition of highly crystallized Ni^{II}–Cr^{III} LDHs in air, to characterize the demixing through the segrega-

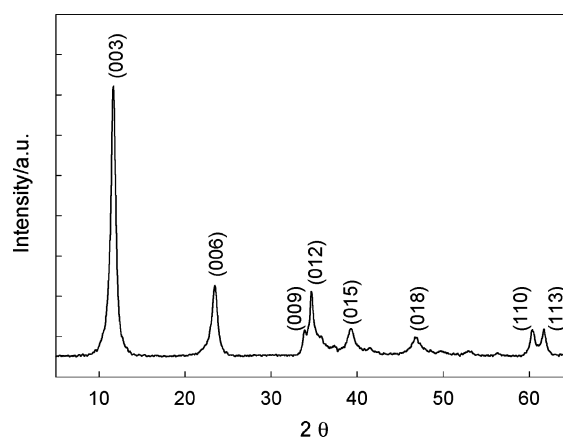


Figure 1. Indexed PXRD pattern of the starting LDH.

tion of metastable nonstoichiometric solid phases. The similarities and differences compared to related systems are discussed.

2. Experimental Section

2.1. Synthesis of LDH. The layered Ni^{II}–Cr^{III} hydroxide was synthesized following the procedure outlined earlier.^{23,24} This involves aging a Cr(NO₃)₃–Ni(NO₃)₂–urea solution in a commercial microwave digester at 493 K for 60 min; the composition of the solution was 0.02 M Cr(NO₃)₃, 0.044 M Ni(NO₃)₂, and 0.5 M urea. The solid was separated by centrifugation, washed with water, and dried in vacuo at room temperature. Its composition, assessed by chemical analysis, was Ni_{0.69}Cr_{0.31}(OH)₂(CO₃)_{0.155}·*n*H₂O. Its PXRD pattern (Figure 1) indicates that the sample is a pure LDH phase.

2.2. Thermal Treatments. Successive thermal treatments were performed in a Shimadzu TGA-51 instrument, under air flow (20 mL min⁻¹). In the first thermal cycle, the Ni^{II}–Cr^{III} LDH was heated from room temperature to 723 K (*T_i*) at a rate of 10 K min⁻¹; once *T_i* was attained, the temperature was kept constant for 30 min, and then, the sample was allowed to cool

* Corresponding authors. E-mail: sileo@qi.fcen.uba.ar (E.E.S.), jobbag@qi.fcen.uba.ar (M.J.).

† Universidad de Buenos Aires.

‡ Universidade Estadual Paulista.

§ Comisión Nacional de Energía Atómica.

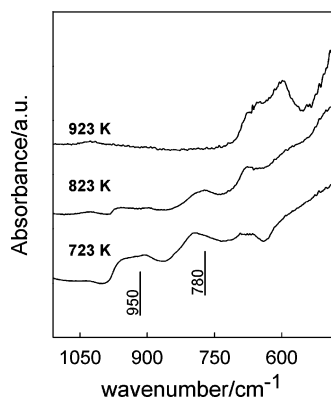


Figure 2. FTIR spectra of the samples annealed in air at different temperatures.

back to room temperature. In the subsequent cycles, the sample was heated to T_i at 20 K min^{-1} and then at 10 K min^{-1} from T_i to the next desired temperature (T_{i+1}), which was kept constant for another 30 min. After each cycle, the samples were analyzed by PXRD and Fourier transform infrared (FTIR).

PXRD patterns were recorded in a Siemens D5000 diffractometer with a Bragg–Brentano geometry, using $\text{Cu K}\alpha$ radiation; generator settings were 40 kV and 30 mA. Divergence, scattered, and receiving radiation slits were 1° , 1° , and 0.2 mm, respectively. A curved graphite monochromator was used. Data were collected in the $16.000^\circ \leq 2\theta \leq 140.000^\circ$ range, with variable scanning steps and counting times. The step width of each run assured a minimum of about twelve intensity points for the narrower peaks. Crystallite size and strain were calculated taking into account the instrument broadening function that was determined using NIST SRM 660 lanthanum hexaboride (LaB_6) standard.

Transmission FTIR spectra of the samples were collected in a Nicolet 510 spectrometer.

2.3. Data Analysis. PXRD data were analyzed by the Rietveld refinement method²⁵ using the GSAS²⁶ routine. The Thompson–Cox–Hasting pseudo-Voigt function,²⁷ with the microstrain broadening description of Stephens,²⁸ was used for fitting the peak profiles. A polynomial function was employed for fitting the background signal. Cell parameters, sample displacement, full width at half-maximum, microstrain broadening, scale factor, and positional parameters for all atoms were refined. The isotropic thermal parameters were fixed at the values measured for an NiO single crystal.²⁹ The preferred orientation in the sample heated at 1773 K was corrected using the March model.³⁰ Only Lorentzian and Gaussian coefficients of peak profiles were refined to obtain the respective crystallite size and microstrain parameters.

3. Results and Discussion

Thermogravimetric analyses (Supporting Information) show that the thermal decomposition of $\text{Ni}_{0.69}\text{Cr}_{0.31}(\text{OH})_2(\text{CO}_3)_{0.155} \cdot n\text{H}_2\text{O}$ occurs in three main steps, as expected for a carbonate-containing LDH.^{31,32} In the first two regions (298–450 K, and 450–580 K), the mass loss is associated with the release of superficial and interlamellar water, respectively; from the second step, $n = 0.64 \text{ mol/mol}$ is derived. The third stage (580–780 K) corresponds to the irreversible decomposition of the LDH, a process in which the evolution of CO_2 overlaps the dehydroxylation of the structure.³³ According to previous reports,^{34,35} Cr^{III} ions are oxidized to Cr^{VI} within the temperature range. Figure 2 shows the IR spectrum of the sample annealed at 723 K, which shows bands at 780 and 950 cm^{-1} that are charac-

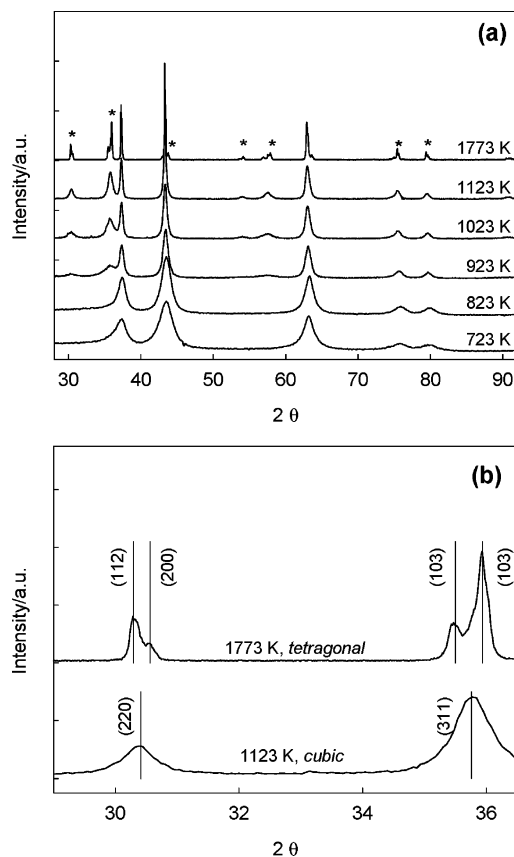


Figure 3. (a) PXRD patterns of the samples annealed in air at increasing temperatures; the asterisks denote the peaks corresponding to the spinel phase. (b) Zoom showing the cubic to tetragonal transition of the spinel phase.

teristic of $\text{Cr}^{\text{VI}}\text{—O}$ vibrations.³⁵ These bands fade with increasing annealing temperature, becoming negligible at 923 K. The trend reveals the reduction of the previously formed Cr^{VI} back to Cr^{III} . In line, the TG trace (cf. Supporting Information) shows a slight weight loss between 800 and 900 K, which corresponds to the elimination of O_2 according to the general stoichiometry $2\text{CrO}_3 \rightarrow \text{Cr}_2\text{O}_3 + \frac{3}{2}\text{O}_2$.

PXRD patterns of the samples annealed at different temperatures are presented in Figure 3A. All of them show the presence of bunsenite. The formation of M^{III} -doped NiO at this relatively low temperature was also reported for the thermal decomposition of $\text{Ni}_{0.70}\text{Co}_{0.30}(\text{OH})_2(\text{CO}_3)_{0.15} \cdot 0.67\text{H}_2\text{O}$.³⁶ At 923 K, nickel chromite is already detected. In agreement with a previously reported work,³⁵ no peaks corresponding to NiCrO_4 are observed in any of the samples annealed below 923 K, thus indicating that Cr^{VI} is well-dispersed within the oxidic matrix; in the case of the $\text{Mg}^{\text{II}}\text{—Cr}^{\text{III}}$ LDH, on the other hand, segregation of MgCrO_4 was observed.³⁵ Figure 3A also indicates changes in the cell parameter and crystallite size of both bunsenite and spinel phases, which are denoted by the variations in the position and width of the diffraction peaks. At 1773 K (Figure 3B), the splitting of the peaks corresponding to nickel chromite indicates a clear change in the crystallographic structure of the spinel phase.

The PXRD patterns of the solids annealed within 723–1123 K can, in principle, be described using two different structural models. In the first one, proposed by Gazzano et al.,³⁷ the changes in the patterns are ascribed to a single-phased NiO super cell ($Fd3m$, where Cr^{III} ions are randomly distributed only in octahedral positions) that modifies its site occupancies with temperature; the nucleation and growth of the spinel phase are

TABLE 1: Agreement Factors and Lattice Cell Parameters for the Refined Samples^a

<i>T</i> /K	<i>a</i> Bn/Å	strain Bn	<i>a</i> Sp/Å	<i>c</i> Sp/Å	GofF	<i>R</i> _{wp}	<i>R</i> _p	<i>R</i> _B	wt % Bn
723	4.1539(6)	1.25			1.28	3.47	2.56	2.30	100
823	4.1541(2)	1.24			1.51	5.04	3.93	3.00	100
923	4.1657(3)	1.11	8.332(1)		1.34	6.71	5.19	3.40	65(1)
1023	4.1692(2)	1.04	8.3234(7)		1.38	7.52	5.77	3.27	60(1)
1123	4.1748(2)	0.85	8.3174(9)		1.38	8.16	5.84	3.75	56(1)
1773	4.1758(1)	0.32	5.8520(1)	8.4014(3)	1.36	11.02	8.52	4.77	53(1)

^a Strain for the NiO-like phase is also shown. Bn = bunsenite. Sp = spinel. $R_p = 100 \sum |I_o - I_c| / \sum I_o$. $R_{wp} = 100 [\sum w_i (I_o - I_c)^2 / \sum w_i I_o^2]^{0.5}$. $R_B = 100 \sum |I_{ko} - I_{kc}| / \sum I_{ko}$. $GofF = \sum w_i (I_o - I_c)^2 / (N - P)$. I_o and I_c = observed and calculated intensities. w_i = weight assigned to each step intensity. I_{ko} and I_{kc} = observed and calculated intensities for Bragg *k*-reflection. N and P = number of data points in the pattern and number of parameters refined. Cell parameters for pure NiO, cubic NiCr₂O₄, and tetragonal NiCr₂O₄ are 4.1758(1), 8.3155(7), and 5.8369(4), 8.4301(6), respectively.

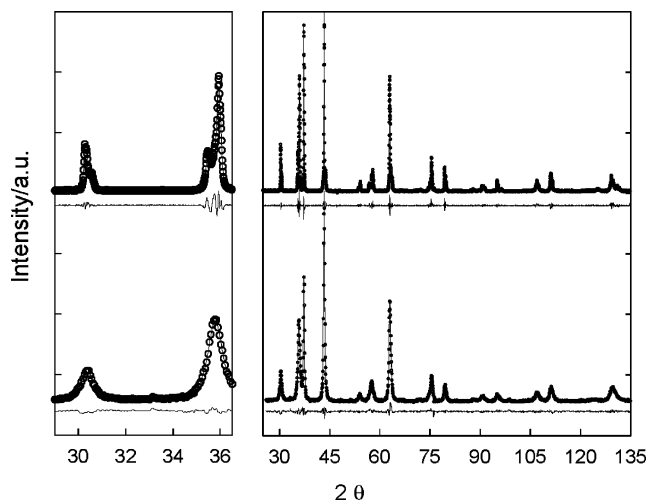


Figure 4. Observed (●) and calculated (solid line) XRD patterns of the samples annealed at 1123 K (lower) and 1773 K (upper); the difference plots are also shown.

viewed as the passing of Ni^{II} from octahedral to tetrahedral sites. Despite the close relationship that exists between the structures of NiO and cubic NiCr₂O₄, this model is unable to fit the present data; no unique peak profile function that could simulate all the diffraction peaks could be found, even though they were corrected for anisotropic line-broadening. The peaks corresponding to the spinel phase are always broader than those of bunsenite, indicating the existence of two different crystallographic phases and the formation of NiCr₂O₄ via a nucleation and growth mechanism.

The second structural model considers that the PXRD patterns of the solids heated at 723 and 823 K correspond to NiO with Cr^{III} ions distributed in octahedral sites, whereas those of the samples heated at $T \geq 923$ K correspond to a biphasic crystallographic system composed of bunsenite and a spinel phase. This model describes the experimental patterns excellently. Figure 4 presents the observed, calculated, and difference PXRD profiles for the samples annealed at 923 and 1123 K. Table 1 collects the indicators of the goodness of the fits, as well as structural information for the various samples; the quality of the refinements is similar for all samples.

The PXRD pattern of the sample heated at 1773 K, in which NiCr₂O₄ only presents its tetragonal variety, was simulated using the *Fm3m* and *I41/amd* spatial groups (Figure 4). The change from cubic to tetragonal, taking place within the range 1123–1773 K, is clearly seen in the blowup presented in Figure 4.

The evolution of the refined cell parameters *a* (for bunsenite) and *a*/*2* (for the spinel) in the range 723–1123 K is presented in Table 1; reported values for pure NiO and cubic NiCr₂O₄ are also included for comparison. The cell parameter of the

bunsenite phase increases with temperature, whereas that of the spinel decreases, both tending toward those reported for the pure phases.

Bunsenite is the only crystalline phase that is produced by thermal decomposition of Ni_{0.69}Cr_{0.31}(OH)₂(CO₃)_{0.155}·0.64H₂O at 723 and 823 K. Within this temperature range, other LDHs evolve into doped bunsenites and an amorphous phase that is richer in the trivalent metal ion.^{38–40} In the present case, the possible presence of an amorphous solid precludes establishing the actual composition of the bunsenite phase. However, the large contraction of the *a* parameter, the high strain (Table 1), and the evident presence of Cr^{VI} (Figure 2) and absence of NiCrO₄ indicate that the formed bunsenite is highly defective, with a rather high degree of chromium doping, with Cr^{III} occupying octahedral sites and Cr^{VI} located probably at the particles surface (cf. ref. 41). In iron-doped bunsenites, Fe^{III} and Fe^{IV} occupy tetrahedral positions.^{42,43}

According to Del Arco et al.,³⁸ upon annealing Ni_{0.7}Fe_{0.3}-(OH)₂(CO₃)_{0.15}·*n*H₂O at 723 K, most of the iron segregates from NiO and forms an amorphous solid in which Fe^{III} adopts the tetrahedral coordination. Likewise, heating of Ni_{0.72}Al_{0.28}(OH)₂(CO₃)_{0.14}·*n*H₂O at 923 K produces a mixture of Al^{III}-doped bunsenite and amorphous Ni^{II}-doped alumina.³⁹ These results seem to contradict our former conclusion. However, the dissimilar thermal behavior of these LDHs is in line with the energetic requirements associated with the transfer of a trivalent metal ion from an octahedral site to a tetrahedral one; the electronic configuration of the 3d³ Cr^{III} ions, which stabilizes the octahedral coordination,⁴⁴ renders a much higher barrier for the diffusion jumps, thus hindering the expulsion of Cr^{III} from the NiO lattice.

At 923 K, where Cr^{VI} is quantitatively reduced (Figure 2), homogeneous nucleation of cubic nickel chromite takes place (Figure 3A). As suggested by Chen et al.,⁴⁵ the very close matching of NiO and NiCr₂O₄ lattices must ease this process. Indeed, the data in Table 1 show that the value of the cell parameter of the spinel phase doubles that of the parent bunsenite, indicating that nucleation of the cubic nickel chromite involves the redistribution of cations within a common framework of oxo ions. The driving force for nucleation and growth is the high Cr^{III} supersaturation of the bunsenite phase; the reported Cr^{III} solubility data span from 1% to 10% in the range 1100–1800 K;^{46–48} these values are much lower than the chromium content of our sample. These two factors should account for the rather low temperature required to produce the spinel phase; for example, the analogous Ni_{0.72}Al_{0.28}(OH)₂(CO₃)_{0.14}·*n*H₂O yields NiAl₂O₄ above 1173 K.⁴⁹

As the temperature is increased, the cell parameters of the bunsenite and the spinel phases shift in opposite ways (Table 1). The contraction of the cell of nickel chromite is compatible with a relative enrichment in the smallest Cr^{III} ions. On the other hand, the expansion of bunsenite and the strain reduction reflect

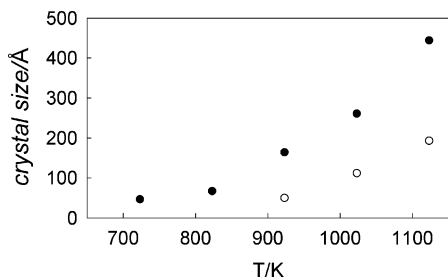


Figure 5. Crystal sizes of the bunsenite (●) and spinel phases (○) as a function of the annealing temperature.

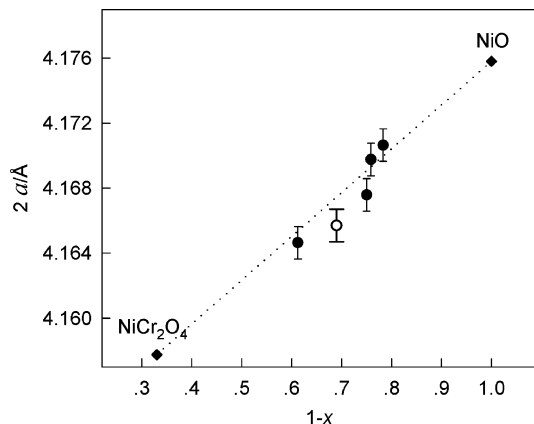


Figure 6. Cell parameters of a family of $\text{Ni}_{1-x}\text{Cr}_x\text{O}_{1+x/2}$ bunsenites as a function of the Ni^{II} content in the parent LDHs: (○) this work; (●) data taken from ref 24. Cell parameters for NiO and cubic NiCr_2O_4 are also included.

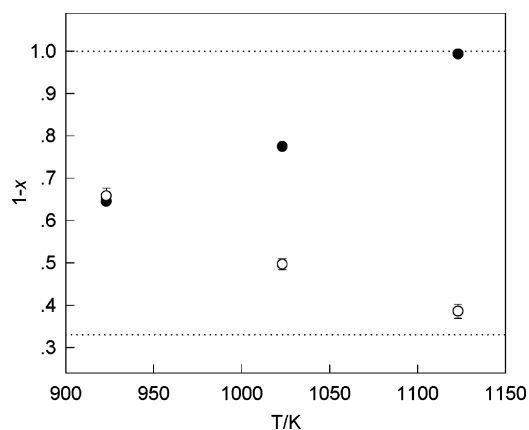


Figure 7. Changes in the Ni^{II} content in the bunsenite (●) and the spinel (○) phases in the 923–1123 K temperature range.

the depletion in Cr^{III} . Both processes occur simultaneously, and the two crystalline phases grow, although at different paces (see Figure 5).

Previously reported information²⁴ shows that the cell parameters of $\text{Ni}_{1-x}\text{Cr}_x\text{O}_{1+x/2}$ bunsenites obtained upon the annealing of $\text{Ni}^{\text{II}}-\text{Cr}^{\text{III}}$ LDHs at 923 K in air obey Vegard's law when presented as a function of the overall LDHs composition; NiO and cubic NiCr_2O_4 were taken as the end members of the series. Likewise, nonstoichiometric spinels obtained from $\text{Zn}^{\text{II}}-\text{Cr}^{\text{III}}$,^{50,51} $\text{Ni}^{\text{II}}-\text{Al}^{\text{III}}$,⁵² and $\text{Co}^{\text{II/III}}-\text{Cr}^{\text{III}}$ ⁵³ double hydroxides observed the same behavior. Our data fall well within the reported trend (Figure 6).

Figure 7 plots the content of Ni^{II} in the bunsenite and spinel phases as a function of the annealing temperature; Ni^{II} contents were derived assuming that both crystalline phases comply with Vegard's law. Interestingly, when nucleation of the spinel takes

place, the cation mole fraction of both phases is almost equal to that of the starting solid. At 1123 K, the cell parameters reveal almost stoichiometric NiCr_2O_4 and NiO phases. Their weight fractions correspond to those expected from the composition of the starting LDH (see Table 1), indicating that demixing is almost completed.

Finally, upon annealing at 1773 K, the spinel phase adopts the tetragonal structure, which is the stable form at room temperature. Clearly, the metastable cubic NiCr_2O_4 phase is stabilized by surface energy, owing to the nanometric size of the crystallites.⁵⁴ The transition from cubic to tetragonal takes place readily, once the size of the parent crystallites reaches a certain critical value.⁵⁵

4. Conclusions

This work illustrates that Rietveld refinement of XRD data of mixtures of double oxides gives sound structural information that enables the characterization of the whole demixing. The method rules out the possible occurrence of a single-phased NiO super cell at the very early stages of the process and indicates that the bunsenite and spinel phases coexist after nucleation of the latter. Formation of nonstoichiometric cubic spinel takes place at 923 K; at this point, the O^{2-} frameworks of both crystalline phases are coincident. Then, cation migration leads to segregation. Once redistribution of cations is completed, the cell parameters of the final crystalline phases are very close to those of the stoichiometric phases. At 1773 K, cubic NiCr_2O_4 transforms into tetragonal NiCr_2O_4 .

Comparison with related systems indicates that the demixing of the parent M^{III} -doped bunsenite phases is governed by the electronic configuration of M^{III} , which determines the path by which nucleation of the spinel phase takes place. In the case of mobile M^{III} ions, nucleation occurs at bunsenite/amorphous solid interfaces. In the case of the sluggish Cr^{III} , on the other hand, homogeneous nucleation takes place in the bulk of Cr^{III} -supersaturated bunsenites. The latter process is further favored by the structural matching of NiO and NiCr_2O_4 .

Supporting Information Available: Thermogravimetric analyses. This material is available free of charge via the Internet at <http://pubs.acs.org>.

Acknowledgment. Support from ANPCyT (PICT 06-06631) is gratefully acknowledged. A.E.R. and M.J. are members of CONICET. M.J. is also a Gabbo's fellow.

References and Notes

- (1) Cavani, F.; Trifirò, F.; Vaccari, A. *Catal. Today* **1991**, *11*, 173.
- (2) Reichle, W. T. *J. Catal.* **1985**, *94*, 547.
- (3) Kusnetsova, T. F.; Burdovitsyna, L. I. *Appl. Catal., A* **1997**, *152*, 6.
- (4) Dufour, L. C.; El Anssari, A.; Dofour, P.; Vareille, M. *Surf. Sci.* **1992**, *269/270*, 1173.
- (5) Kooli, F.; Rives, V.; Ulibarri, M. A. *Inorg. Chem.* **1996**, *35*, 5313.
- (6) Rao, C. N. R. *Reactivity of Solids: Past, Present and Future*; Boldyrev, V. V., Ed.; IUPAC Chemistry for the XXIst Century Series; Blackwell Science: Oxford, 1996.
- (7) Spinolo, G.; Anselmi-Tamburini, U. *J. Phys. Chem.* **1989**, *93*, 6837.
- (8) Xu, Z. P.; Zeng, H. C. *Chem. Mater.* **2000**, *12*, 3459.
- (9) Petrov, K.; Zotov, N.; Mirtcheva, E.; García Martínez, O.; Rojas, R. M. *J. Mater. Chem.* **1994**, *4*, 611.
- (10) Zeng, H. C.; Xu, Z. P. *Chem. Mater.* **1998**, *10*, 2277.
- (11) Xu, Z. P.; Zeng, H. C. *Chem. Mater.* **1999**, *11*, 67.
- (12) Del Arco, M.; Rives, V.; Trujillano, R.; Malet, P. *J. Mater. Chem.* **1996**, *6*, 1419.
- (13) Kooli, F.; Rives, V.; Ulibarri, M. A. *Inorg. Chem.* **1995**, *34*, 5114.
- (14) Yun, S. K.; Pinnavaia, T. J. *Inorg. Chem.* **1996**, *35*, 6853.
- (15) Alejandre, A.; Medina, F.; Salagre, P.; Correig, X.; Sueiras, J. E. *Chem. Mater.* **1999**, *11*, 939.

- (16) Rives, V.; Kannan, S. *J. Mater. Chem.* **2000**, *10*, 489.
- (17) Kagunya, W.; Hassan, Z.; Jones, W. *Inorg. Chem.* **1996**, *35*, 5970.
- (18) Morpurgo, S.; Lo Jacono, M.; Porta, P. *J. Mater. Chem.* **1994**, *4*, 197.
- (19) Morpurgo, S.; Lo Jacono, M.; Porta, P. *J. Solid State Chem.* **1995**, *119*, 246.
- (20) Liu, J.; Li, F.; Evans, D. G.; Duan, X. *Chem. Commun.* **2000**, 542.
- (21) Belloto, M.; Rebours, B.; Clause, O.; Lynch, J.; Bazin, D.; Elkaïm, E. *J. Phys. Chem.* **1996**, *100*, 8535.
- (22) Clause, O.; Gazzano, M.; Trifirò, F.; Vaccari, A.; Zatorski, L. *Appl. Catal.* **1991**, *73*, 217.
- (23) Jobbágy, M.; Regazzoni, A. E. in *Proceedings of the Sixth International Symposium on Hydrothermal Reactions*; Yanagisawa, K., Feng, Q., Eds.; Nishimura Tosha-Do, Ltd.: Kochi, Japan, 2001; pp 373–376.
- (24) Jobbágy, M. Ph.D. Thesis, Universidad de Buenos Aires, 2003.
- (25) Rietveld, H. M. *J. Appl. Crystallogr.* **1969**, *2*, 65.
- (26) Larson, A. C.; Von Dreele, R. B. *General Structure Analysis System (GSAS)*; Los Alamos National Laboratory Report LAUR 86-748; U.S. Government Printing Office: Washington, DC, 1994.
- (27) Thompson, P.; Cox, D. E.; Hastings, J. B. *J. Appl. Crystallogr.* **1987**, *20*, 79.
- (28) Stephens, P. W. *J. Appl. Crystallogr.* **1999**, *32*, 281.
- (29) Geller, S.; Wood, E. A. *Acta Crystallogr.* **1956**, *9*, 563.
- (30) Dollase, W. A. *J. Appl. Crystallogr.* **1986**, *19*, 267.
- (31) Hudson, M. J.; Carlino, S.; Apperley, D. C. *J. Mater. Chem.* **1995**, *5*, 323.
- (32) Constantino, V. R. L.; Pinnavaia, T. J. *Inorg. Chem.* **1995**, *34*, 883.
- (33) Rives, V. *Inorg. Chem.* **1999**, *38*, 406.
- (34) Fuda, K.; Suda, K.; Matsunaga, T. *Chem. Lett.* **1993**, 1479.
- (35) Labajos, F. M.; Rives, V. *Inorg. Chem.* **1996**, *35*, 5313.
- (36) Vaysse, C.; Guerlou-Demourgues, L.; Delmas, C. *Inorg. Chem.* **2002**, *41*, 6905.
- (37) Gazzano, M.; Kagunya, W.; Matteuzzi, D.; Vaccari, A. *J. Phys. Chem. B* **1997**, *101*, 4514.
- (38) Del Arco, M.; Malet, P.; Trujillano, R.; Rives, V. *Chem. Mater.* **1999**, *11*, 624.
- (39) Rebours, B.; d'Espinose de la Caillerie, J. B.; Clause, O. *J. Am. Chem. Soc.* **1994**, *116*, 1707.
- (40) Jobbágy, M.; Soler-Illia, G. J. A. A.; Regazzoni, A. E.; Blesa, M. A. *Chem. Mater.* **1998**, *10*, 1632.
- (41) Giamello, E.; Fubini, E.; Bertoldi, M.; Busca, G.; Vaccari, A. *J. Chem. Soc., Faraday Trans. 1* **1989**, *85*, 237.
- (42) Haass, F.; Buhrmester, T.; Martin, M. *Phys. Chem. Chem. Phys.* **2001**, *3*, 4806.
- (43) Haass, F.; Buhrmester, T.; Martin, M. *Solid State Ionics* **2001**, *141*, 289.
- (44) Dunitz, J. D.; Orgel, L. E. *J. Phys. Chem. Solids* **1957**, *3*, 318.
- (45) Chen, C.; Notis, M. R.; Williams, D. B. *J. Am. Ceram. Soc.* **1983**, *66*, 566.
- (46) Greskovich, G. *J. Am. Ceram. Soc.* **1970**, *53*, 498.
- (47) Słoczynski, J.; Kowalski, Z.; Wójcikiewicz, T. *Bull. Acad. Pol. Sci. XX* **1972**, *11–12*, 1097.
- (48) Hirschwald, W.; Loechel, B.; Nowotny, J.; Oblakowski, J.; Sikora, I.; Stolze, F. *Bull. Acad. Pol. Sci. XXIX* **1982**, *7–8*, 369.
- (49) Clause, O.; Rebours, B.; Merlen, E.; Trifirò, F.; Vaccari, A. *J. Catal.* **1992**, *133*, 231.
- (50) Bertoldi, M.; Bice, F.; Giamello, E.; Busca, G.; Trifirò, F.; Vaccari, A. *J. Chem. Soc., Faraday Trans. 1* **1988**, *84*, 1405.
- (51) Riva, A.; Trifirò, F.; Vaccari, A.; Mintchev, L.; Busca, G. *J. Chem. Soc., Faraday Trans. 1* **1988**, *84*, 1423.
- (52) Busca, G.; Lorenzelli, V.; Sanchez Escribano, V. *Chem. Mater.* **1992**, *4*, 595.
- (53) Busca, G.; Trifirò, F.; Vaccari, A. *Langmuir* **1990**, *6*, 1440.
- (54) Pottier, A.; Cassaignon, S.; Chanéac, C.; Villain, F.; Tronc, E.; Jolivet, J. P. *J. Mater. Chem.* **2003**, *13*, 877.
- (55) Crottaz, O.; Kubel, F.; Schmid, H. *J. Mater. Chem.* **1997**, *7*, 143.